

## **Distribution Agreement**

In presenting this thesis as a partial fulfillment of the requirements for a degree from Emory University, I hereby grant to Emory University and its agents the non-exclusive license to archive, make accessible, and display my thesis in whole or in part in all forms of media, now or hereafter known, including display on the World Wide Web. I understand that I may select some access restrictions as part of the online submission of this thesis. I retain all ownership rights to the copyright of the thesis. I also retain the right to use in future works (such as articles or books) all or part of this thesis.

Syed K. Mehdi

04/17/13

The Regulation of Base Excision Repair: The Effects of Sumoylation on Ntg1 Function

by

Syed K. Mehdi

Paul Doetsch  
Advisor

Department of Biology

Paul Doetsch  
Advisor

Gray Crouse  
Committee Member

Karla Passalacqua  
Committee Member

2013

The Regulation of Base Excision Repair: The Effects of Sumoylation on Ntg1 Function

by

Syed K. Mehdi

Paul Doetsch

Advisor

An abstract of a thesis submitted  
to the Faculty of the Emory College of Arts and Sciences of  
Emory University in partial fulfillment of the requirements  
of the degree of Bachelor of Science with Honors

Department of Biology

2013

## Abstract

### The Regulation of Base Excision Repair: The Effects of Sumoylation on Ntg1 Function

By Syed K. Mehdi

Unrepaired oxidative damage to DNA leads to the development of cancer and other degenerative diseases. The cellular mechanism base excision repair (BER) ensures proper repair of damaged DNA in both the nucleus and mitochondria. Unfortunately, not a great deal of information is known about the regulation of this crucially important mechanism. The BER protein of *Saccharomyces cerevisiae*, Ntg1, which is post-translationally modified by sumoylation, dynamically localizes to either the nucleus or mitochondria upon cellular increases in oxidative DNA damage. While the phenomenon of dynamic localization is understood, the mechanism of Ntg1 regulation in repairing a diverse range of lesions in the nucleus and mitochondria is unknown. I propose that sumoylation of Ntg1, by a small ubiquitin like modifying protein (SUMO), will regulate Ntg1 function by driving dynamic localization to areas of oxidative DNA damage, and/or altering its enzymatic activity. In order to observe whether sumoylation of Ntg1 altered its dynamic localization and/or its enzymatic activity, it was first necessary to produce artificial SUMO fusion proteins. Localization of one fusion protein was observed under standard growth conditions and upon introduction of oxidative DNA damage using fluorescence microscopy. Enzymatic activity of the other fusion protein, when introduced to a dihydrouracil substrate, was observed using an enzyme assay. Our results indicate sumoylated Ntg1 shares the same localization pattern as wild type Ntg1 under standard growth conditions and upon introduction to oxidative DNA damage. Similarly, the Ntg1 SUMO fusion possesses comparable enzymatic activity with wild type Ntg1 towards a dihydrouracil containing substrate. Overall, these results are significant in the understanding of the role of sumoylation in the regulation of a vital DNA repair mechanism in base excision repair. Further study of this sumoylation regulation pathway is necessary if we are to understand how base excision repair is not only regulated in *Saccharomyces cerevisiae*, but ultimately in humans as well. By studying and understanding the regulation of BER in yeast, we will be able to further understand how DNA repair is regulated in humans, and possibly discover new methods of fighting cancer.

The Regulation of Base Excision Repair: The Effects of Sumoylation on Ntg1 Function

by

Syed K. Mehdi

Paul Doetsch

Advisor

A thesis submitted to the Faculty of the Emory College of Arts and Sciences  
of Emory University in partial fulfillment  
of the requirements of the degree of  
Bachelor of Science with Honors

Department of Biology

2013

## Acknowledgements

I would like to acknowledge Dan Swartzlander, my lab mentor, for helping me grow as a scientist. I would like to acknowledge Dr. Paul Doetsch, my research advisor, for providing me with invaluable advice and support. I would like to thank Nick Bauer for taking the time to run my experiments through his Q-SCAN program. Finally, I would like to acknowledge all the members of the Doetsch lab for their encouragement and suggestions as this project was completed. I could not have accomplished my goals without their wisdom.

## Table of Contents

BACKGROUND.....	1
MATERIALS AND METHODS.....	4
RESULTS.....	8
DISCUSSION.....	12
REFERENCES.....	17
FIGURES AND TABLES LEGENDS.....	19
TABLES	
1. Strains and Plasmids.....	24
2. Averaged Results of Localization Scoring by Visualization.....	24
FIGURES	
1. Model of the base excision repair pathway.....	25
2. Model of Sumoylation.....	25
3. Locations of Putative Consensus SUMO Modification Sites on Ntg1.....	26
4. Hypothetical Model of Sumoylated Ntg1 Localization and Enzymatic Activity.....	26
5. Localization of Ntg1-GFP and Ntg1-Smt3-GFP Under Standard Growth Conditions....	27
6. Averaged Results for Localization Scoring by Visualization and Localization Scoring by Q-SCAN program.....	27
7. Western Blot of Ntg1-Smt3-His and Controls with and without IPTG Induction.....	28
8. SDS Gel of Nickel and FPLC Purifications of Ntg1-Smt3-His6 and Controls.....	29
9. Western Blot of Nickel and FPLC Purifications of Ntg1-Smt3-His6.....	30
10. SDS Gel of Ntg1-Smt3-His6 After Adjusting Purification.....	30
11. Western Blot of Ntg1-Smt3-His6 After Adjusting Purification.....	31
12. Western Blot of Modified Purifications of Ntg1-Smt3-His6 and Controls.....	32
13. Typhoon Image of Elution 1 and Elution 1 Concentrate of Ntg1-Smt3-His6 and Controls.....	33
14. Typhoon Image of Ntg1-Smt3-His6 Enzymatic Activity Assay.....	33
15. Quantification Results of Ntg1-Smt3-His6 Enzymatic Activity Assay.....	34

## **Background**

DNA that is damaged by endogenous sources such as reactive oxidative species (ROS), and exogenous sources such as UV radiation, when left unrepaired, leads to cancer, and other degenerative diseases(1,2). ROS, which cause oxidative DNA damage in the nucleus and the mitochondria, are one of the main sources of cellular DNA damage(3,4). One source of endogenous ROS is normal cellular metabolism that uses oxygen for oxidative phosphorylation in the mitochondria(5). ROS cause DNA damage in both the nucleus and mitochondria. DNA lesions that are produced as a result of oxidative DNA damage are repaired through different evolutionary conserved pathways such as single-strand break repair and base excision repair(3,4).

The main DNA repair pathway utilized to repair oxidative DNA damage is the base excision repair (BER) pathway. *N*-glycosylases initiate BER by removing damaged bases from DNA forming apurinic/apyrimidinic sites. Apurinic/apyrimidinic (AP) sites are locations in the DNA that lack a purine or pyrimidine(6,7). These sites are created by *N*-glycosylase activity, as a result of spontaneous hydrolysis of the *N*-glycosylic bond in DNA, and from chemical agents and radiation(6-9). After the creation of an AP site, the DNA backbone is cleaved on either the 5' side by an AP endonuclease, or on the 3' side by an AP lyase(10). Once the blocking groups, which consist of either a 5'- deoxyribosephosphate (5'-dRP) or a 3'- dRP, are processed, the DNA template is restored by DNA polymerase and DNA ligase(10) (Figure 1). While the activity of BER proteins is understood, the methods by which they are regulated when the cell is exposed to DNA damage are still widely unknown. In order to study the regulation of BER, I utilized the bifunctional *N*-glycosylase/AP lyase BER protein Ntg1 in *Saccharomyces cerevisiae*. This yeast BER protein is homologous to the human BER protein NTHL1(11).

Ntg1 has two activities: it recognizes oxidative DNA damage, creating an AP site by removing the damaged base, and it also functions as an AP lyase, creating a nick in the DNA backbone on the 3' side of the AP site(12). Ntg1 possesses both a nuclear localization signal and a mitochondrial matrix targeting sequence allowing Ntg1 localization to both the nucleus and mitochondria under normal growth conditions(13-16). Upon DNA damage, Ntg1 dynamically relocates either to the nucleus or mitochondria, depending upon the location and level of the damage, where it initiates BER to maintain genomic stability(13-16). The dynamic localization of Ntg1 to the mitochondria and nucleus is hypothesized to be caused by mitochondrial oxidative DNA damage signals (MODDS) and nuclear oxidative DNA damage signals (NODDS), respectively(17). While it is clear that Ntg1 dynamically localizes to the nucleus or mitochondria following DNA damage, it is still unknown how Ntg1 is regulated to do so. One proposed mechanism of this regulation is the sumoylation of Ntg1 which occurs through addition of a SUMO (Small Ubiquitin-like Modifier) protein.

SUMO proteins covalently attach to other proteins and cause an alteration in the target proteins function. Sumoylation of proteins is a post-translational modification that impacts many crucial cellular functions. SUMO modification occurs in proteins that perform tasks such as regulating gene expression, tumor suppression, maintaining DNA stability, nuclear-cytosolic transport, and apoptosis(18). Sumoylation occurs via a three enzyme pathway that resembles the ubiquitination pathway(19) (Figure 2). First, the SUMO protein is cleaved by the Ulp1 SUMO protease to expose the C-terminal glycine-glycine motif. The SUMO protein is then conjugated to the E1 SUMO activating protein, an Uba2/ Aos1 heterodimer, through a thioester bond(20). The SUMO protein is then transferred to the E2 conjugating protein, Ubc9, through a thioester bond(20). The conjugated E2 protein then, along with the E3 SUMO ligase, attaches the SUMO

protein onto the epsilon amine on lysine on the substrate(20). One major difference between sumoylation and ubiquitination is the amount of different E3 ligases present(20). While ubiquitination has more than 20, there are only four E3 ligases in *Saccharomyces cerevisiae*, Siz1, Siz2, Mms21, and Zip3(20,21). Another unique difference between sumoylation and ubiquitination in *S. cerevisiae*, is the ability of the E2 protein to attach the SUMO protein onto the substrate without the presence of the E3 ligase(20,21). Sumoylation can be reversed due to the SUMO proteases Ulp1 and Ulp2(20). Ulp1 is associated with the desumoylation of mono-sumoylated sites and Ulp2 is associated with the desumoylation of a polySUMO chain(22). SUMO proteins are normally conjugated to a SUMO consensus site on the substrate protein consisting of  $\Psi$ KXE/D, where  $\Psi$  consists of a bulky aliphatic residue, and X donates any amino acid residue(22) (Figure 3).

The SUMO pathway is a highly conserved process present in both *S. cerevisiae* and humans. In order to study the effects of sumoylation on BER in higher organisms such as humans, I have studied Smt3, the SUMO protein in the model eukaryote *S. cerevisiae*. Smt3 is an integral part of maintaining chromosomal integrity throughout mitosis(23,24). There are five major SUMO consensus sumoylation sites on Ntg1. These sites are located at K20, K38, K376, K388, and K396 (Unpublished, Swartzlander). I will study how sumoylation modifies Ntg1 function by testing whether it plays a role in dynamically relocating Ntg1 to sites of DNA damage as well as altering its enzymatic activity.

My goal in this project is to not only observe how dynamic relocation of Ntg1 to organelles containing oxidative DNA damage is regulated, but also to observe how Ntg1 sumoylation affects the *N*-glycosylase and AP lyase activities of Ntg1. In order to accomplish these goals, I will employ an Ntg1-Smt3-GFP fusion protein as well as an Ntg1-Smt3-His6

fusion protein. The GFP tag will be used to observe where sumoylated Ntg1 localizes in the absence of DNA damage, and where it dynamically relocates following oxidative stress. The His6 fusion will be used to observe any alteration in the enzymatic activity of Ntg1 upon sumoylation. Specifically, I will study whether sumoylation of Ntg1 causes the loss or alteration of either AP lyase or *N*-glycosylase functions. My overall hypothesis is that sumoylation of the BER protein Ntg1 will change its enzymatic activity and/or where it localizes in *S. cerevisiae* following exposure to oxidative DNA damage (Figure 4).

## **Materials and Methods**

### **Strains, Media, and Growth Conditions**

All haploid strains of *S. cerevisiae* and all plasmids used in this study are listed in Table 1. Yeast cells were grown at 30°C in YPD medium (1% yeast extract, 2% peptone, 2% dextrose, 0.005% adenine sulfate, and 2% agar was used for plates). Strains of *E. coli* were grown at 37°C in Luria Broth (1% bacto-tryptone, 0.5% yeast extract, 1% sodium chloride) with ampicillin (100µg/uL)(LB-Amp).

### **Plasmid Construction**

To create the Ntg1-Smt3-GFP fusion, the pD0338 plasmid that already contains the *NTG1-GFP* genes was used. The pD0338 plasmid uses the pPS904 backbone that is a 2-micron multicopy plasmid containing the *URA3* gene. The wild type *SMT3* gene from the DSC0295 strain of *S. cerevisiae* was amplified using polymerase chain reaction. The gene was then inserted into the pD0338 backbone using the XhoI restriction site between the *NTG1* gene and the *GFP* gene. The plasmid fusion construct was then transformed into *S. cerevisiae*.

Already containing the non-integrated Ntg1-Smt3-GFP plasmid, the Q-SCAn plasmid was then integrated into the *S. cerevisiae* chromosomal genome. The Q-SCAn (Quantitative Subcellular Compartmentalization Analysis) plasmid produces an NLS-tdTomato fluorescent protein and an MTS-Cerulean fluorescent protein (Unpublished, Bauer). Using Q-SCAn, a program developed by fellow lab member Nick Bauer, the fluorescence of the tdTomato and cerulean proteins, which mark the nucleus and mitochondria respectively, was utilized to quantify the fluorescence of the GFP protein localized in the nucleus and mitochondria. Every cell in each image was then given a score correlated to the average intensity of GFP in the nucleus and mitochondria. A score of zero indicates complete mitochondrial localization and a score of one indicates complete nuclear localization.

To create the Ntg1-Smt3-His6 fusion, the pET-15b plasmid that contains the *NTG1* gene and a His6 tag was used. This plasmid contains the *lac* promoter, which is inducible with IPTG, as well as the Amp<sup>R</sup> gene for ampicillin (Amp) resistance selection. The *NTG1-SMT3* genes from our other plasmid were amplified with primers that included the His6 sequence. *NTG1-SMT3-HIS6* was then inserted into the pET-15b backbone using the XbaI and BamHI restriction sites and transformed into the BL21 (DE3) strain of *Escherichia coli*.

### Protein Purification

Nickel chromatography was utilized for protein purification of wild type Ntg1-His6, Ntg1-Smt3-His6, and *ntg1<sub>cat</sub>*-His6 proteins. *E. coli* BL21 (DE3) containing the plasmids was grown in 5 ml of Luria broth with ampicillin (100µg/uL) (LB-Amp) overnight at 37°C. 1 ml of the overnight culture was added to 100 ml of LB-Amp and grown overnight at 37°. 50 ml of the overnight culture was added to 1L LB-Amp and grown for ~ 2-3 hours until an OD600 of 0.5-1.0 was achieved. Protein expression was then induced for 4 hours at 25°C by the addition of 1 mM

isopropyl  $\beta$ -D-thiogalactoside (IPTG). The cells were then lysed via sonication, and the supernatant applied to a  $\text{Ni}^+$  affinity chromatography (Qaigen) to purify each protein. After three washes with nickel wash buffer (50 mM  $\text{KH}_2\text{PO}_4$ , 300 mM KCl, and 20 mM Imidazole at a pH of 8.0) and three elutions with nickel elution buffer (50 mM  $\text{KH}_2\text{PO}_4$ , 300 mM KCl, and 300 mM Imidazole at a pH of 8.0) the elutions were pooled together, dialyzed overnight in 2L of buffer A, and further purified by an anion exchange FPLC (Pharmacia) with two buffers, buffer A (20 mM  $\text{KH}_2\text{PO}_4$ , 10% glycerol, 0.5 mM EDTA, 1 mM DTT, and 100 mM KCl at a pH of 7.4) and buffer B (20 mM  $\text{KH}_2\text{PO}_4$ , 10% glycerol, 0.5 mM EDTA, 1 mM DTT, and 1000 mM KCl at a pH of 7.4).

#### Exposure to DNA Damaging Agents

The DSC0282 strain of *Saccharomyces cerevisiae* cells containing the Q-SCAn plasmid and either the Ntg1-GFP or Ntg1-Smt3-GFP plasmid was inoculated in 5 ml of YPD media or SD –URA media (0.17% yeast nitrogen base, 0.5% ammonium sulfate, 2% dextrose, and 0.005% adenine sulfate) and grown to  $5 \times 10^7$  cells/ml, centrifuged, washed with water, and resuspended in 5 ml of water. These cells were then left untreated, treated with 20 mM  $\text{H}_2\text{O}_2$  (Sigma) or treated with 20 mM  $\text{H}_2\text{O}_2$  and 10  $\mu\text{g/ml}$  antimycin (Sigma) and incubated for 1 hour at 30°C.

#### Fluorescence Microscopy

Once cells were either left untreated or exposed to DNA damaging agents as described above, they were analyzed by direct fluorescence confocal microscopy utilizing a Zeiss LSM510 META microscope and Carl Zeiss LSM Image Browser software. To quantify Ntg1-Smt3-GFP localization, cells were evaluated for nuclear only, mitochondrial only, or nuclear and mitochondrial localization. Standard deviations for three experimental repeats were calculated for each treatment condition.

### SDS-PAGE

10% SDS-gels composed of water, 30% acrylamide mix, 1.5 M Tris (pH 8.8), 10% SDS, 10% ammonium persulfate, and TEMED were utilized to observe expression of the Ntg1-Smt3-His6 protein. Coomassie blue was used to stain the SDS-gels and visualize protein (0.1% Coomassie R250, 10% acetic acid, and 40% methanol).

### Western Blot

Western blot analysis was performed, according to standard protocols, to evaluate proper protein expression. The primary antibody used was a mouse monoclonal anti-polyhistidine-peroxidase (1:2,000 dilution) (Sigma-Aldrich) to detect the histidine tag on the purified proteins. The secondary antibody used for the Typhoon imager was the Cy5 anti-Rabbit (1:2,000 dilution) (GE Life Sciences). Imagequant TL was utilized to quantify the Typhoon images.

### Enzyme Assay

To assess the enzymatic activity of the purified proteins, an oligonucleotide containing dihydrouracil at position 13 (DHU-31mer) was purchased from Midland Certified Reagent Company. A complementary strand containing a guanine opposite the dihydrouracil was purchased from Eurofins MWG/Operon. The DHU-31mer was labeled on the 5' end with [ $\gamma$ -<sup>32</sup>P] ATP (Amersham) and T4 polynucleotide kinase (Promega) prior to annealing to the complementary strand(25). The single-stranded DHU-31mer was annealed in a 1:1.6 molar ratio to a complementary strand. It was heated to 80°C for 10 minutes and cooled down to room temperature. DNA strand scission assays were performed in 20  $\mu$ l of standard reaction buffer containing 100 mM KCl, 10mM Tris-HCl, pH 7.5, 1 mM EDTA, 50 fmol of labeled DNA substrate and 20 fmol of Ntg1-Smt3-His6 protein. This reaction was performed at 37°C for 30 minutes. The reaction was stopped by the addition of 10  $\mu$ l of loading buffer comprised of 90%

formamide, 1 mM EDTA, 0.1% xylene cyanol and 0.1% bromophenol blue. The reaction products were heated at 90°C for 5 minutes and then resolved on a 15% denaturing PAGE gel and analyzed with a Typhoon Imager (GE Life Sciences).

## Results

There were two main goals of this project. This first goal was to study how dynamic localization of the BER protein Ntg1 to organelles containing oxidative DNA damage was regulated. The second goal was to observe if and how sumoylation of Ntg1 affected its *N*-glycosylation and AP lyase functionality. In order to study sumoylated Ntg1 localization, localization of wild type Ntg1-GFP and Ntg1-Smt3-GFP, when left untreated, was compared. Also, dynamic localization of Ntg1-GFP and Ntg1-Smt3-GFP was assessed by visual analysis and compared to localization scoring accomplished by Nick Bauer's Q-SCAN program (Materials and Methods). To study the enzymatic activity of sumoylated Ntg1, Ntg1-Smt3-His6 was induced, purified through nickel affinity chromatography, concentrated, and an enzyme assay was performed.

### Ntg1-Smt3-GFP Localization Under Standard Growth Conditions

For DNA visualization in untreated wild type Ntg1-GFP and Ntg1-Smt3-GFP cells, cell cultures were incubated with 1 µg/ml DAPI for five minutes. Using direct fluorescence confocal microscopy, it was observed that Ntg1-Smt3-GFP localized to the nuclei and mitochondria sharing the same base localization pattern as Ntg1-GFP under standard growth conditions (Figure 5). Due to the artificial nature of the SUMO fusion, it is possible that Smt3 is simply being dragged to wherever Ntg1 is localizing, as desumoylation cannot occur. Because there was no change in localization of Ntg1-Smt3-GFP compared to wild type Ntg1 under standard growth

conditions, the dynamic localization profile of Ntg1-Smt3-GFP in response to oxidative DNA damage was assayed.

#### Ntg1-Smt3-GFP Localization Upon Introduction of Oxidative DNA Damage

Three trials were performed and localization scoring was performed both visually and using the Q-SCAN program. While three trials were performed, only two were used to calculate the average and standard deviation. This is because in the third trial, a large number of cells were unscorable by visualization for both conditions due to the inability to determine the location or presence of a nucleus, reducing the respective sample sizes to cells ranging from 30 to 65 cells. Similarly, a majority of the images were deemed unscorable by the Q-SCAN program for trial three.

When the averages were taken for the first two trials a few trends appeared. For wild type, when scoring by visualization, there was an increase in mitochondrial only localization from untreated to the two treatments (23.54% to 39.66% for H<sub>2</sub>O<sub>2</sub> and 36.90% for both H<sub>2</sub>O<sub>2</sub> and antimycin A) and a decrease in mitochondrial and nuclear localization (68.32% to 52.53% for H<sub>2</sub>O<sub>2</sub> and 58.38% for both H<sub>2</sub>O<sub>2</sub> and antimycin A) (Table 2). For Ntg1-Smt3-GFP, when scoring by visualization, there was also an increase in mitochondrial only localization from untreated to the two treatments (16.19% to 33.09% for H<sub>2</sub>O<sub>2</sub> and 38.79% for both H<sub>2</sub>O<sub>2</sub> and antimycin A) and a decrease in mitochondrial and nuclear localization (78.65% to 61.62% for H<sub>2</sub>O<sub>2</sub> and 59.05% for both H<sub>2</sub>O<sub>2</sub> and antimycin A). For the Q-SCAN averages, for wild type, the average index for the three conditions was 0.635, 0.569 for H<sub>2</sub>O<sub>2</sub>, and 0.550 for H<sub>2</sub>O<sub>2</sub> and antimycin A, again indicating increased mitochondrial localization when exposed to oxidative DNA damage (Figure 6). For Ntg1-Smt3-GFP, the average index for the three conditions was 0.704, 0.700 for H<sub>2</sub>O<sub>2</sub>, and 0.562 for H<sub>2</sub>O<sub>2</sub> and antimycin A. Both scoring by visualization and with the Q-SCAN

program indicates an increase in mitochondrial localization upon exposure to oxidative stress for both wild type Ntg1 and Ntg1-Smt3-GFP. The Smt3 fusion on Ntg1 does not appear to change its dynamic localization when compared to the wild type Ntg1-GFP (Table 2 and Figure 6).

Previously published work demonstrated an increase in nuclear localization and a decrease in mitochondrial localization in Ntg1-GFP upon exposure to H<sub>2</sub>O<sub>2</sub>(17). In the published experiment, however, the OD of the yeast cells was never measured so the growth rate was unknown. This may have led to variability each time the experiment was performed. Also, the yeast cells in the published experiment did not contain the Q-SCAn plasmid. These factors may have contributed to the disparity in the control results.

#### Protein Induction and Purification

Prior to purification of Ntg1-Smt3-His6 it was necessary to determine that the Smt3 fusion construct was the correct size and was inducible with IPTG. A Western blot indicates that Ntg1-Smt3 is the expected size (lane 4) and able to be induced with IPTG (lanes 3 and 4) (Figure 7). The Western blot also indicates that the positive control Ntg1-His6 and the negative control *ntg1<sub>cat</sub>*-His6 are inducible with IPTG (Figure 7).

Once it was determined the Ntg1-Smt3-His6 plasmid was properly constructed and inducible, it was necessary to purify the protein using nickel affinity purification and FPLC (Fast Phase Liquid Chromatography). The purification of both controls, Ntg1-His6 and *ntg1<sub>cat</sub>*-His6, proceeded normally (Figure 8A,B). Unfortunately, Ntg1-Smt3-His6 did not purify as expected by nickel ion-exchange chromatography as indicated by the lack of protein in the elutions and, as a result, there was no purification from this FPLC step (Figure 8C). To determine whether Ntg1-Smt3-His6 was present in the purification but below the level of detection by Coomassie staining, Western blot analysis was performed. The Western blot revealed that some Ntg1-Smt3

bound and eluted from the nickel column in the first elution, as well as in the early FPLC fractions (Figure 9). The presence of protein in the early FPLC fractions indicates poor binding of the Ntg1-Smt3-His6 protein to the sulfopropyl column (Figure 9). There was also a great deal of degraded products in nickel elution 1 and the early FPLC fractions. To address the degradation issue, the incubation time of the Ntg1-Smt3-His6 protein on nickel beads was reduced from overnight to two hours and the dialysis time for the FPLC purification was reduced from overnight to two hours. For the sulfopropyl column binding issue, the pH of the FPLC buffer solutions was changed from 7.4 to 6.4. At a pH of 7.4, Ntg1-Smt3-His6 was negatively charged which would hinder binding to the anion exchange SP column. At a pH of 6.4, however, Ntg1-Smt3-His6 was positively charged and equal to that of Ntg1-His6 at pH 7.4.

Using the new conditions, another protein purification of Ntg1-Smt3-His6 was performed. The new purification indicated increased binding and elution with the nickel column but the FPLC purification failed to yield purified protein (elution 1, Figure 10). Western blot analysis also indicated protein in elution 1, but there was still no binding to the SP column and there was a great deal of degradation products (Figure 11). As a result of the failed FPLC purification it was decided that nickel affinity purification alone would yield sufficiently pure Ntg1-Smt3-His6 to use in enzyme assays. Wild type Ntg1-His6 and *ntg1<sub>cat</sub>*-His6 were also purified in this manner. (Figures 12A-C).

#### Ntg1-Smt3 Enzymatic Activity Assay

After obtaining partially purified proteins, the ability of Ntg1-Smt3-His6 to excise dihydrouracil (DHU) from an oligonucleotide and cleave the DNA backbone was assessed by fellow lab member Dan Swartzlader. In order to have equal molar ratios of wild type Ntg1, Ntg1-Smt3 and *ntg1<sub>cat</sub>*, significantly more total protein lysate was required from the partially purified

Ntg1-Smt3 sample (Figure 13). As expected, the pure purified wild type Ntg1 cleaved the oligonucleotide containing DHU, and the amount of cleavage product increased as the amount of protein increased. Similarly, *ntg1<sub>cat</sub>* had no enzymatic activity and there was minimal presence of cleavage product. Ntg1-Smt3 produced a cleavage product similar to that of wild type Ntg1, and increasing the amount of Ntg1-Smt3 protein led to a reduction in uncleaved DNA (Figure 14). Every lane, including Ntg1-Smt3, had a smaller band present under the major cleavage product. In the Ntg1-Smt3 lanes, however, there were significantly larger amounts of smaller cleavage products. This could be accounted for by the fact that a significantly larger amount of partially purified protein was used to load similar molar ratios of Ntg1 for the Ntg1-Smt3 samples. Those extra bands may have occurred due to the cleavage activity of other exonucleases in the partially purified Ntg1-Smt3 lysate. In order to account for those smaller cleavage products when quantifying the cleavage assay, the smaller bands were added to the major cleavage product for all of the protein samples. Quantification indicated that in both the wild type Ntg1 and Ntg1-Smt3, the percent of DHU cleaved increased as the amount of protein added increased (Figure 15). Overall, the partially purified Ntg1-Smt3-His6 appeared to have comparable enzymatic activity to wild type Ntg1. It appears the artificial SUMO fusion on the Ntg1 C-terminus does not disrupt Ntg1 enzymatic activity towards repairing dihydrouracil DNA damage.

### **Discussion**

Base excision repair is crucial for the maintenance of genomic stability in both the nucleus and mitochondria. While research has been performed to understand the mechanism of BER focusing on the enzymes involved and their activity in the overall pathway, very little is known about its regulation. This research project helps answer some of those questions by

studying the yeast SUMO protein Smt3, a potential regulatory protein of the BER protein Ntg1. We focused on the impact of sumoylation on the localization and enzymatic activity of Ntg1 when exposed to reactive oxygen species, a common source of endogenous DNA damage in humans. We found that when Smt3 is fused to Ntg1 to simulate sumoylation, the localization patterns of the wild type Ntg1-His6 and Ntg1-Smt3-His6 fusion are similar under both standard growth conditions and when exposed to oxidative DNA damage. We also found that, similar to wild type Ntg1, the Smt3 fusion protein can successfully cleave an oligonucleotide containing dihydrouracil indicating that Ntg1-Smt3-His6 has comparable enzymatic activity to wild type Ntg1. Since BER is crucial for maintenance of genomic stability, we anticipate that this data will provide a better understanding of a potential regulatory component of this pathway.

#### Wild Type Ntg1-GFP and Ntg1-Smt3-GFP Share Localization Patterns Under Standard Growth Conditions and Upon Introduction of Oxidative DNA Damage

When exposed to oxidative DNA damage, both wild type Ntg1-GFP and Ntg1-Smt3-GFP exhibited similar localization patterns. Both increased localization to the mitochondria. I was unable to reproduce previously published work from the Doetsch lab as my results indicated that upon exposure to oxidative stress, wild type Ntg1-GFP increased mitochondrial only localization and decreased nuclear only localization. Interestingly though, when analyzing the Q-SCAN program results, there appeared to be a slight increase in mitochondrial only localization when wild type Ntg1-GFP was exposed to oxidative DNA damage. In the published work, however, localization scoring was never performed using the Q-SCAN program. It is possible that Q-SCAN allows for more accurate localization scoring than scoring by visualization using DAPI and Mitotracker to denote the nucleus and mitochondria respectively. On the other hand, the Q-SCAN tdTomato and mCerulean proteins may be negatively influencing localization scoring by

affecting GFP localization. Under standard growth conditions, however, Ntg1-Smt3-GFP appears to share the same localization as wild type Ntg1-GFP. This may be accounted for by the fact that we are using an Ntg1-Smt3-GFP fusion protein. This fusion consists of Smt3 fused to the last amino acid of Ntg1, lysine 399, with a four amino acid linker sequence between. Unpublished data from the lab indicates lysine 396 on Ntg1 is the primary site of monosumoylation (Unpublished, Swartzlander). Whereas normal sumoylation occurs on a side chain, the artificial fusion of Smt3 forms a peptide bond with amino acid 399 on Ntg1. Due to the artificial and irreversible nature of the Smt3 fusion, the localization of Ntg1-Smt3-GFP to the nucleus or mitochondria may simply be a byproduct of Ntg1 dragging the Smt3 portion of the protein along with it. Additional issues we faced with the Ntg1-GFP and Ntg1-Smt3-GFP dynamic localization experiments was overall weak fluorescence that made scoring by visualization very difficult, particularly in the treated samples. In order to alleviate this issue, yeast cells that are near an optical density of 3.0 will be used as these cells are near the end of log phase growth. Currently, yeast cells at an optical density of 2.0 are being used. At this phase of growth it is likely that these cells are still dividing, causing many to die when exposed to H<sub>2</sub>O<sub>2</sub> or H<sub>2</sub>O<sub>2</sub> and antimycin A, which ultimately leads to weak fluorescence and may have led to the differences in the published work and our control.

#### Wild type and Sumoylated Ntg1 Possess Comparable Enzymatic Activities for Dihydrouracil Substrates

While Ntg1-His6 had been successfully purified with both nickel affinity chromatography and fast phase liquid chromatography, the purification of the artificial SUMO fusion protein encountered many challenges. First, there was a significant amount of protein degradation that occurred. Since this is a fusion protein, it may have appeared as foreign to the

cell, in which case the cell attempted to degrade the protein. Even in the presence of protease inhibitors and a reduction in length of certain components of the purifications, protein degradation remained a significant issue. Since the cells were lysed via sonication before nickel purification, it is possible that the lysing of the cells led to a biological response to degrade the cellular proteins. When observing the SDS gels by Coomassie or Western blots, protein degradation seemed to begin after the post-clear, or sonication, step (Figure 11). Along with degradation, column binding was another major issue that arose. While wild type Ntg1-His6 had no issue binding to the sulfopropyl column used in the FPLC purification, the artificial SUMO was unable to bind. Even after altering the pH of the buffer solutions, no binding occurred to the SP column. Due to all these issues, I decided to perform only nickel purifications as SDS gels and Western blots indicated there was partially purified Ntg1-Smt3-His6 in the first elutions (Figure 9, 10 & 11). Despite these issues, I was able to concentrate the partial purifications and use them to observe the enzymatic activity of Ntg1-Smt3-His6. As the enzyme assay indicated, the Ntg1-Smt3-His6 fusion had the ability to cleave an oligonucleotide containing a dihydrouracil substrate. Along with the ability to cleave this damaged oligonucleotide, it appears the fusion protein possesses similar enzymatic activity when compared to the wild type Ntg1-His6. The significance of this result is that it shows the Ntg1-Smt3 fusion possesses similar enzymatic activity as wild type Ntg1. It is believed that sumoylation is a major component in Ntg1 regulation and localization. One potential role of sumoylation may be to regulate the concentration of Ntg1 in the cell. The concentrations of various BER proteins are delicately balanced in a cell. An uncontrolled increase in concentration of one protein would affect the entire BER pathway. In order to prevent this, one biological role of sumoylation may be protein degradation. It is also likely that the enzymatic activity of Ntg1 is regulated through sumoylation.

It was possible that Ntg1 activity could have been reduced or its substrate specificity altered by a change in the active site conformation due to sumoylation. Our results, however, indicate that Ntg1 activity is in fact not diminished when sumoylated and when exposed to an oligonucleotide possessing a dihydrouracil. In my hypothesis, I believed sumoylation would impact the dynamic localization and/or enzymatic activity of Ntg1. These results indicate that Ntg1-Smt3-GFP has similar localization to Ntg1-GFP under both standard growth conditions and upon introduction of oxidative DNA damage. They also show Ntg1-Smt3-His6 has comparable enzymatic activity to Ntg1-His6 when exposed to a dihydrouracil substrate. While localization of Ntg1-Smt3-GFP was similar to wild type, the SUMO fusion may still be regulating Ntg1. Also, while Ntg1-Smt3-His6 has comparable enzymatic activity to wild type Ntg1 for a dihydrouracil substrate, it may differ in activity towards different types DNA damage. The next step in this project, then, is to explore sumoylated Ntg1 activity when exposed to other types of DNA damage such as abasic sites. We will investigate the potentially varying specificity and enzymatic activity of sumoylated Ntg1 towards one type of DNA damage over another. Overall, these results are significant in the complete understanding of the role of sumoylation in not just protein regulation as whole, but specifically regulation of a vital DNA repair mechanism in base excision repair. Further studying of this sumoylation regulation pathway is necessary if we are to understand how base excision repair is not only regulated in *Saccharomyces cerevisiae*, but ultimately in humans as well.

### References

1. Polyak, K., Li, Y., Zhu, H., Lengauer, C., Willson, J.K., Markowitz, S.D., Trush, M.A., Kinzler, K.W. and Vogelstein, B. (1998) Somatic mutations of the mitochondrial genome in human colorectal tumours. *Nat Genet*, **20**, 291-293.
2. Kujoth, G.C., Hiona, A., Pugh, T.D., Someya, S., Panzer, K., Wohlgemuth, S.E., Hofer, T., Seo, A.Y., Sullivan, R., Jobling, W.A. *et al.* (2005) Mitochondrial DNA mutations, oxidative stress, and apoptosis in mammalian aging. *Science*, **309**, 481-484.
3. Slupphaug, G., Kavli, B. and Krokan, H.E. (2003) The interacting pathways for prevention and repair of oxidative DNA damage. *Mutat Res*, **531**, 231-251.
4. Richter, C., Park, J.W. and Ames, B.N. (1988) Normal oxidative damage to mitochondrial and nuclear DNA is extensive. *Proc Natl Acad Sci U S A*, **85**, 6465-6467.
5. Jamieson, D.J. (1998) Oxidative stress responses of the yeast *Saccharomyces cerevisiae*. *Yeast*, **14**, 1511-1527.
6. Lindahl, T. and Nyberg, B. (1972) Rate of depurination of native deoxyribonucleic acid. *Biochemistry*, **11**, 3610-3618.
7. Lindahl, T. and Andersson, A. (1972) Rate of chain breakage at apurinic sites in double-stranded deoxyribonucleic acid. *Biochemistry*, **11**, 3618-3623.
8. Scharer, O.D. and Jiricny, J. (2001) Recent progress in the biology, chemistry and structural biology of DNA glycosylases. *Bioessays*, **23**, 270-281.
9. Krokan, H.E., Standal, R. and Slupphaug, G. (1997) DNA glycosylases in the base excision repair of DNA. *Biochem J*, **325 (Pt 1)**, 1-16.
10. Boiteux, S. and Guillet, M. (2004) Abasic sites in DNA: repair and biological consequences in *Saccharomyces cerevisiae*. *DNA Repair (Amst)*, **3**, 1-12.
11. Aspinwall, R., Rothwell, D.G., Roldan-Arjona, T., Anselmino, C., Ward, C.J., Cheadle, J.P., Sampson, J.R., Lindahl, T., Harris, P.C. and Hickson, I.D. (1997) Cloning and characterization of a functional human homolog of *Escherichia coli* endonuclease III. *Proc Natl Acad Sci U S A*, **94**, 109-114.
12. Augeri, L., Hamilton, K.K., Martin, A.M., Yohannes, P. and Doetsch, P.W. (1994) Purification and properties of yeast redoxendonuclease. *Methods Enzymol*, **234**, 102-115.
13. Ikeda, S., Kohmoto, T., Tabata, R. and Seki, Y. (2002) Differential intracellular localization of the human and mouse endonuclease III homologs and analysis of the sorting signals. *DNA Repair (Amst)*, **1**, 847-854.
14. Alseth, I., Eide, L., Pirovano, M., Rognes, T., Seeberg, E. and Bjoras, M. (1999) The *Saccharomyces cerevisiae* homologues of endonuclease III from *Escherichia coli*, Ntg1 and Ntg2, are both required for efficient repair of spontaneous and induced oxidative DNA damage in yeast. *Mol Cell Biol*, **19**, 3779-3787.
15. You, H.J., Swanson, R.L., Harrington, C., Corbett, A.H., Jinks-Robertson, S., Senturker, S., Wallace, S.S., Boiteux, S., Dizdaroglu, M. and Doetsch, P.W. (1999) *Saccharomyces cerevisiae* Ntg1p and Ntg2p: broad specificity N-glycosylases for the repair of oxidative DNA damage in the nucleus and mitochondria. *Biochemistry*, **38**, 11298-11306.

16. Griffiths, L.M., Swartzlander, D., Meadows, K.L., Wilkinson, K.D., Corbett, A.H. and Doetsch, P.W. (2009) Dynamic compartmentalization of base excision repair proteins in response to nuclear and mitochondrial oxidative stress. *Mol Cell Biol*, **29**, 794-807.
17. Swartzlander, D.B., Griffiths, L.M., Lee, J., Degtyareva, N.P., Doetsch, P.W. and Corbett, A.H. (2010) Regulation of base excision repair: Ntg1 nuclear and mitochondrial dynamic localization in response to genotoxic stress. *Nucleic Acids Res*, **38**, 3963-3974.
18. Dhananjayan, S.C., Ismail, A. and Nawaz, Z. (2005) Ubiquitin and control of transcription. *Essays Biochem*, **41**, 69-80.
19. Gareau, J.R. and Lima, C.D. (2010) The SUMO pathway: emerging mechanisms that shape specificity, conjugation and recognition. *Nat Rev Mol Cell Biol*, **11**, 861-871.
20. Xu, Z., Chan, H.Y., Lam, W.L., Lam, K.H., Lam, L.S., Ng, T.B. and Au, S.W. (2009) SUMO proteases: redox regulation and biological consequences. *Antioxid Redox Signal*, **11**, 1453-1484.
21. Kerscher, O., Felberbaum, R. and Hochstrasser, M. (2006) Modification of proteins by ubiquitin and ubiquitin-like proteins. *Annu Rev Cell Dev Biol*, **22**, 159-180.
22. Ulrich, H.D. (2008) The fast-growing business of SUMO chains. *Mol Cell*, **32**, 301-305.
23. Geiss-Friedlander, R. and Melchior, F. (2007) Concepts in sumoylation: a decade on. *Nat Rev Mol Cell Biol*, **8**, 947-956.
24. Dasso, M. (2008) Emerging roles of the SUMO pathway in mitosis. *Cell Div*, **3**, 5.
25. Meadows, K.L., Song, B. and Doetsch, P.W. (2003) Characterization of AP lyase activities of *Saccharomyces cerevisiae* Ntg1p and Ntg2p: implications for biological function. *Nucleic Acids Res*, **31**, 5560-5567.
26. Creton, S. and Jentsch, S. (2010) SnapShot: The SUMO system. *Cell*, **143**, 848-848 e841.
27. Rigaut, G., Shevchenko, A., Rutz, B., Wilm, M., Mann, M. and Seraphin, B. (1999) A generic protein purification method for protein complex characterization and proteome exploration. *Nat Biotechnol*, **17**, 1030-1032.

### **Figure and Table Legend**

Figure 1. **Model of the base excision repair pathway (10)**. This figure illustrates which enzymes undergo certain processes of the base excision repair pathway.

Figure 2. **Model of sumoylation (26)**. This figure demonstrates the general sumoylation pathway. It displays the various enzymes in the pathway and their role in each step of sumoylation.

Figure 3. **Location of putative consensus and non-consensus SUMO modification sites on Ntg1**. This figure shows the amino acid sequence of the Ntg1 protein. The mitochondrial targeting sequence is highlighted in yellow, the nuclear localization signal is highlighted in dark blue, and the catalytic site which was mutated as a negative control is highlighted in green. The red lysines are the five major consensus SUMO sites on Ntg1 (Unpublished, Swartzlander). They are K20, K38, K376, K388, and K396

Figure 4. **Hypothetical model of sumoylated Ntg1 localization and enzymatic activity**. This figure was made by me to present the two main goals of this research project. The top half of the model illustrates wild type Ntg1-GFP localization upon exposure to oxidative DNA damage. Ntg1-GFP localizes to areas of DNA damage and initiates DNA repair. The bottom half shows the two goals addressed in this project. The first goal is to observe how Ntg1 localization is impacted upon sumoylation. Sumoylated Ntg1 may have greater localization to the nucleus or mitochondria than wild type Ntg1 upon exposure to oxidative DNA damage. The other goal is to observe if enzymatic activity and enzymatic specificity of Ntg1 is altered upon sumoylation. Sumoylated Ntg1 may have greater affinity than wild type Ntg1 for a certain type of DNA damage.

Figure 5. **Base localization of Ntg1-GFP and Ntg1-Smt3-GFP under standard growth conditions.** In this image, the localization of Ntg1-GFP was assessed via fluorescence microscopy. DAPI (blue) was used to observe DNA localization and GFP (green) was used to observe Ntg1 and Ntg1-Smt3 localization. DAPI compartmentalized nuclear and mitochondrial localization and GFP fluorescence overlay visualized Ntg1 and Ntg1-Smt3 localization in the cell. The merged images of cells expressing wild type Ntg1 and Ntg1-Smt3-GFP are shown and the red squares highlight the nucleus and mitochondria.

Figure 6. **Graphs of averaged results from trial 1 and trial 2 for localization scoring by visualization and localization scoring by the Q-SCAn program.** This figure contains the graphs for the averaged results from trial 1 and trial 2 for the localization experiments.

Localization of Ntg1-GFP and Ntg1-Smt3-GFP to the nuclei only (nuc), mitochondria only (mito) or nuclei and mitochondria (nuc + mito) was determined for each cell and plotted as a percentage of the total scorable cells. The error bars indicate the standard deviation. The graph in panel A is for localization scoring by visualization and the graph in panel B is for localization scoring performed by the Q-SCAn program. A localization index value of 0 corresponds to complete mitochondrial localization and a value of 1 corresponds to complete nuclear localization.

Figure 7. **Western blot of Ntg1-His6, Ntg1-Smt3-His6, and  $ntg1_{cat}$ -His6 protein expression with and without induction by IPTG.** This figure contains the Western blot used to determine that the Ntg1-Smt3-His6 plasmid was successfully constructed, was expressing the desired protein, and was inducible with IPTG. A mouse monoclonal anti-polyhistidine-peroxidase antibody was used. The presence of the darker bands in the +IPTG lane compared to the -IPTG lane in all three conditions indicated that all three plasmids were inducible with IPTG. The larger

band in the +IPTG Ntg1-Smt3-His6 lane compared to the band in the +IPTG Ntg1-His6 lane indicated that the Ntg1-Smt3-His6 plasmid contained the desired SMT3 insert.

**Figure 8. SDS gel of nickel and FPLC purifications of wild type Ntg1-His6, ntg1<sub>cat</sub>-His6, and Ntg1-Smt3-His6.** This figure shows a SDS gel containing the nickel and FPLC purifications of wild type Ntg1 (panel A), ntg1<sub>cat</sub>-His6 (panel B) and Ntg1-Smt3-His6 (panel C). The lanes in the nickel purification were the following: a cell pellet after IPTG induction, pre-sonication sample, post-sonication pellet, post sonication supernatant, flow through containing protein unbound to the nickel column, the flow through from wash 1, wash 2, wash 3, elution 1, elution 2, elution 3, dialysis with the three elutions, and flow through containing protein unbound to the sulfopropyl column used in the FPLC purification. The lanes in the FPLC purification were every 3-4 elution fractions to observe when the desired protein eluted off the sulfopropyl column. No protein purified in the Ntg1-Smt3-His6 purifications.

**Figure 9. Western blot of nickel and FPLC purifications of Ntg1-Smt3-His6.** This figure shows a Western blot containing the nickel and FPLC purifications of Ntg1-Smt3-His6.

Degradation products begin to appear after post-sonication, especially in elution 1, and there is protein only in the first few FPLC fractions. The degradation bands are smaller than 26 kDa.

**Figure 10. SDS gel of nickel and FPLC purification of Ntg1-Smt3-His6 after adjusting purification method.** This figure shows a SDS gel containing purification products for the modified nickel purification of Ntg1-Smt3-His6. This purification was stopped after elution 1. Elution 1 was collected and then concentrated. The faint band around 64 kDa in elution 1 is the Ntg1-Smt3-His6 protein.

**Figure 11. Western blot of nickel and FPLC purification of Ntg1-Smt3-His6 after adjusting purification method.** This figure shows a Western blot containing purification products for the

modified nickel purification of Ntg1-Smt3-His6. This purification was stopped after elution 1. Elution 1 was collected and then concentrated. There are degradation products appearing post-sonication and in elution 1 and there is protein only in the first few FPLC fractions.

**Figure 12. Western blot of modified nickel purification of wild type Ntg1-His6, ntg1<sub>cat</sub>-His6, and Ntg1-Smt3-His6.** This figure shows a Western blot containing purification products for the modified nickel purification of wild type Ntg1-His6, ntg1<sub>cat</sub>-His6, and Ntg1-Smt3-His6. The lanes in the nickel purification were the following: pre-IPTG lysate, a cell pellet after IPTG induction, pre-sonication sample, post-sonication supernatant, flow through containing protein unbound to the nickel column, the flow through from wash 1, wash 2, wash 3, elution 1, elution 2, elution 3, and concentrated elution 1.

**Figure 13. Typhoon image of elution 1 and concentrated elution 1 for wild type Ntg1-His6, Ntg1-Smt3-His6 and ntg1<sub>cat</sub>-His6.** This figure is of a typhoon image of a Western blot of elution 1 and concentrated elution 1 of Ntg1-His6, Ntg1-Smt3-His6, and ntg1<sub>cat</sub>-His6. The higher bands in the Ntg1-Sm3-His6 lane indicate the presence of partially purified Ntg1-Smt3-His6. There is also partially purified wild type Ntg1-His6 and ntg1<sub>cat</sub>-His6. The Ntg1-Smt3-His6 band is lighter than the other two proteins indicating more total protein lysate is required from Ntg1-Smt3-His6 to achieve equal molar ratios of Ntg1 with the other conditions.

**Figure 14. Typhoon image of the Ntg1-Smt3-His6 enzymatic activity assay result.** This figure contains a typhoon image of an enzyme assay performed with Ntg1-Smt3-His6 using a radioactive labeled phosphate on an oligonucleotide containing a dihydrouracil substrate. The lanes in the denaturing page gel were as follows: a negative control with no enzyme, endonuclease III, pure protein samples of wildtype Ntg1, and ntg1<sub>cat</sub> and finally, partially purified protein samples of wildtype Ntg1, Ntg1-Smt3, ntg1<sub>cat</sub>, concentrated wildtype Ntg1, and

concentrated ntg1<sub>cat</sub>. The Ntg1<sub>K5R</sub> strain was not used in my experiment, but it is Ntg1 with all five lysine of the major consensus SUMO sites substituted with arginine. The top bands are the labeled oligonucleotide containing a dihydrouracil substrate and the bottom bands are the cleaved oligonucleotide.

Figure 15. **Quantification results of the Ntg1-Smt3-His6 enzymatic activity assay.** This figure contains a graph that quantifies the percent of dihydrouracil that was cleaved by various amounts of Ntg1-His6, Ntg1-Smt3-His6, and ntg1<sub>cat</sub>-His6 proteins. The small cleavage products that appeared in the denaturing gel were added with the major cleavage product when the percent of overall cleavage was calculated.

Table 1. **Strains and Plasmids used in this study.**

Table 2. **Averaged results of trial 1 and trial 2 for localization scoring by visualization.** This table shows the average percentage of cells that had either Ntg1-GFP or Ntg1-Smt3-GFP localization to the nucleus only (ave nuc), mitochondria only (ave mito) or the nucleus and mitochondria (ave nuc + mito) when exposed to one of three conditions. Cells were left untreated, treated with H<sub>2</sub>O<sub>2</sub> only, or treated with both H<sub>2</sub>O<sub>2</sub> and antimycin A. The average percentage is based on two trials, and the percentages are based on scorable cells only, not total cells.

## Tables

Table 1

Strain or Plasmid	Description	Reference
DSC0282	MATa ura3-52 leu2Δ1 his3Δ200 ntg1::KAN bar1::HYG	(27)
DSC0295	MATa his3Δ1 leu2Δ0 met 15Δ0 ura3Δ0 TET- induced C-terminal TAP tagged NTG1	(16)
DSC0564	MATa ura3-52 leu2Δ1 his3Δ200 ntg1::KAN bar1::HYG, Q-SCAn (nls-tdTomato, mts-Cerulean, LEU)	This study
DSC0565	MATa ura3-52 leu2Δ1 his3Δ200 ntg1::KAN bar1::HYG, Q-SCAn (nls-tdTomato, mts-Cerulean, LEU), pD0338 (Ntg1-GFP)	This study
DSC0566	MATa ura3-52 leu2Δ1 his3Δ200 ntg1::KAN bar1::HYG, Q-SCAn (nls-tdTomato, mts-Cerulean, LEU), pD0462 (Ntg1-Smt3-GFP)	This study
Q-SCAn	<i>p<sub>CYCI</sub>.BPSV40NLS-tdTomato, p<sub>TEF1</sub>.Su9MTS-mCerulean, LEU2,</i>	Bauer, unpublished
pD0338	<i>pPS904, NTG1-GFP, 2μ, URA3, amp<sup>R</sup></i>	This study
pD0390	pET-15b <i>NTG1-His<sub>6</sub>, lacI, amp<sup>R</sup></i>	(18)
pD0394	pET-15b <i>ntg1<sub>catalytic</sub>-His<sub>6</sub>, lacI, amp<sup>R</sup></i>	(18)
pD0462	<i>pPS904, NTG1-SMT3-GFP, 2μ, URA3, amp<sup>R</sup></i>	This study
pD0463	pET-15b <i>NTG1-SMT3-His<sub>6</sub>, lacI, amp<sup>R</sup></i>	This study

Table 2

		Ave Nuc (%)	Ave Mito (%)	Ave Nuc + Mito (%)
Ntg1-GFP	NT	8.15	23.54	68.32
	H <sub>2</sub> O <sub>2</sub>	7.81	39.66	52.53
	HA	4.72	36.9	58.38
Ntg1-Smt3-GFP	NT	5.17	16.19	78.65
	H <sub>2</sub> O <sub>2</sub>	5.3	33.09	61.62
	HA	2.17	38.79	59.05

## Figures

Figure 1

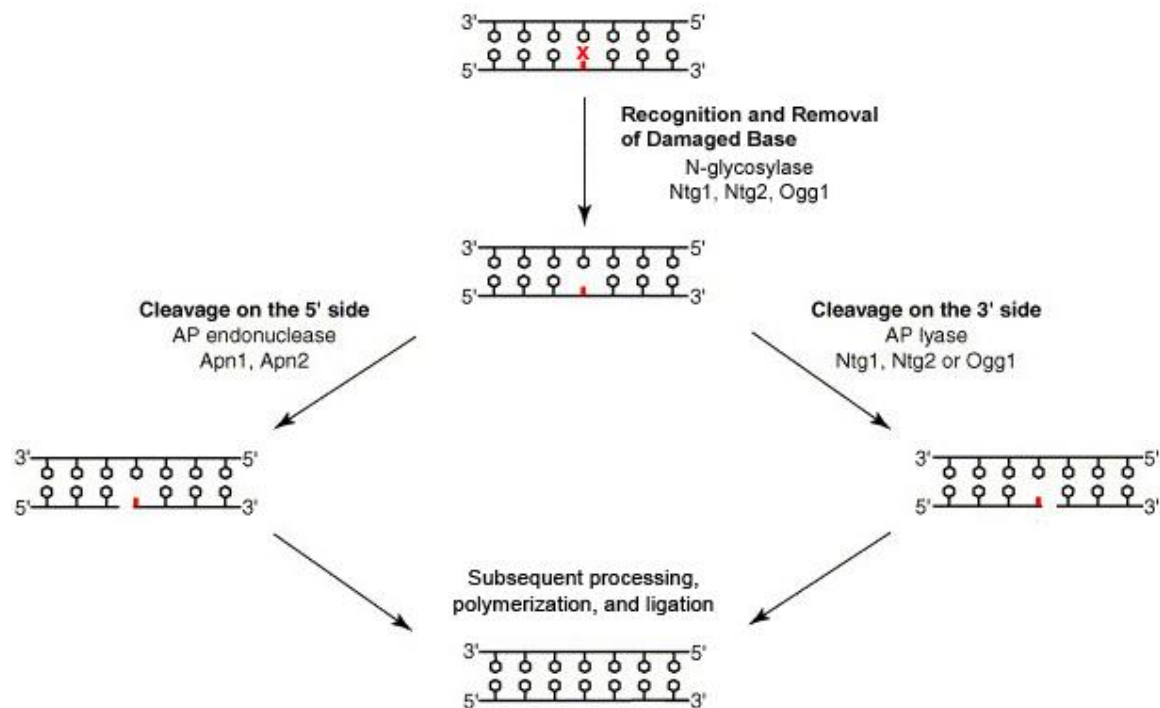


Figure 2

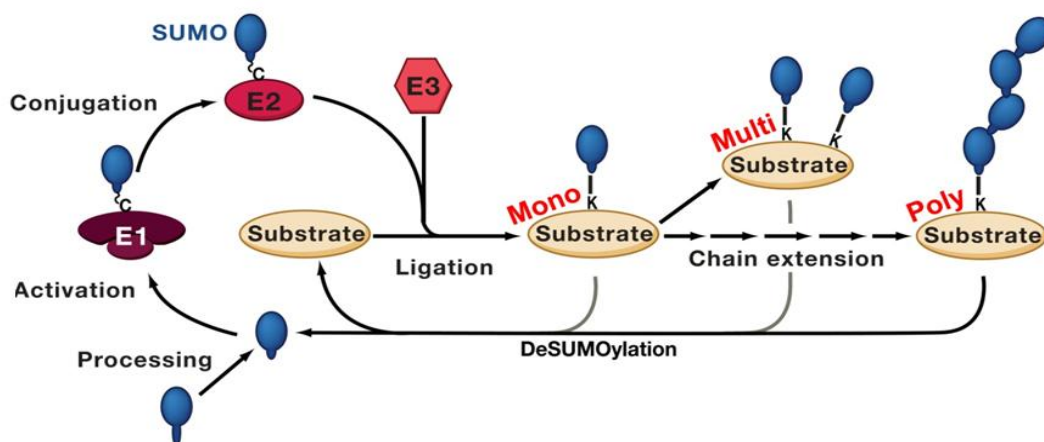


Figure 3

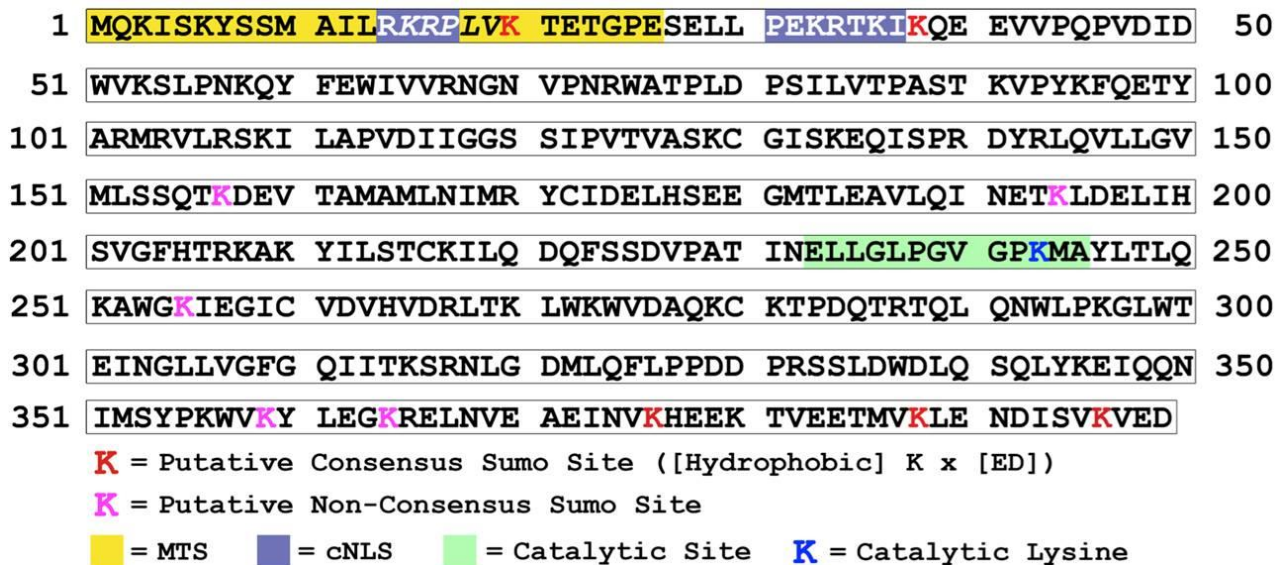


Figure 4

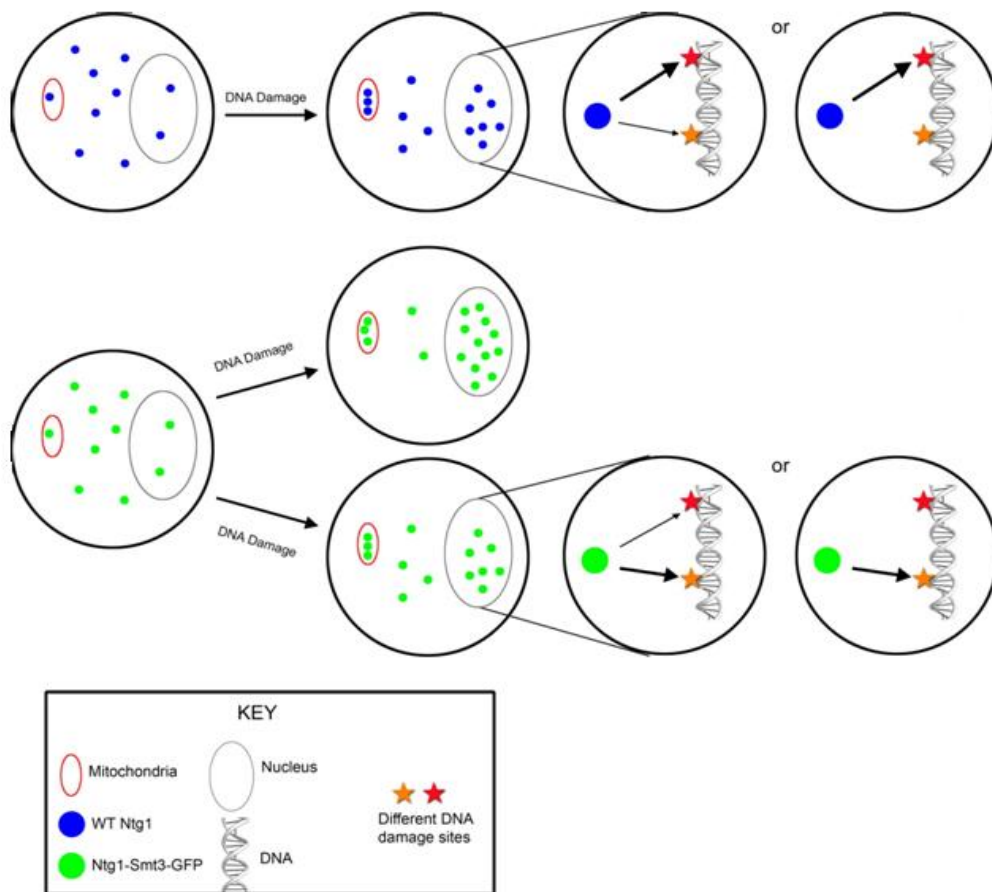


Figure 5

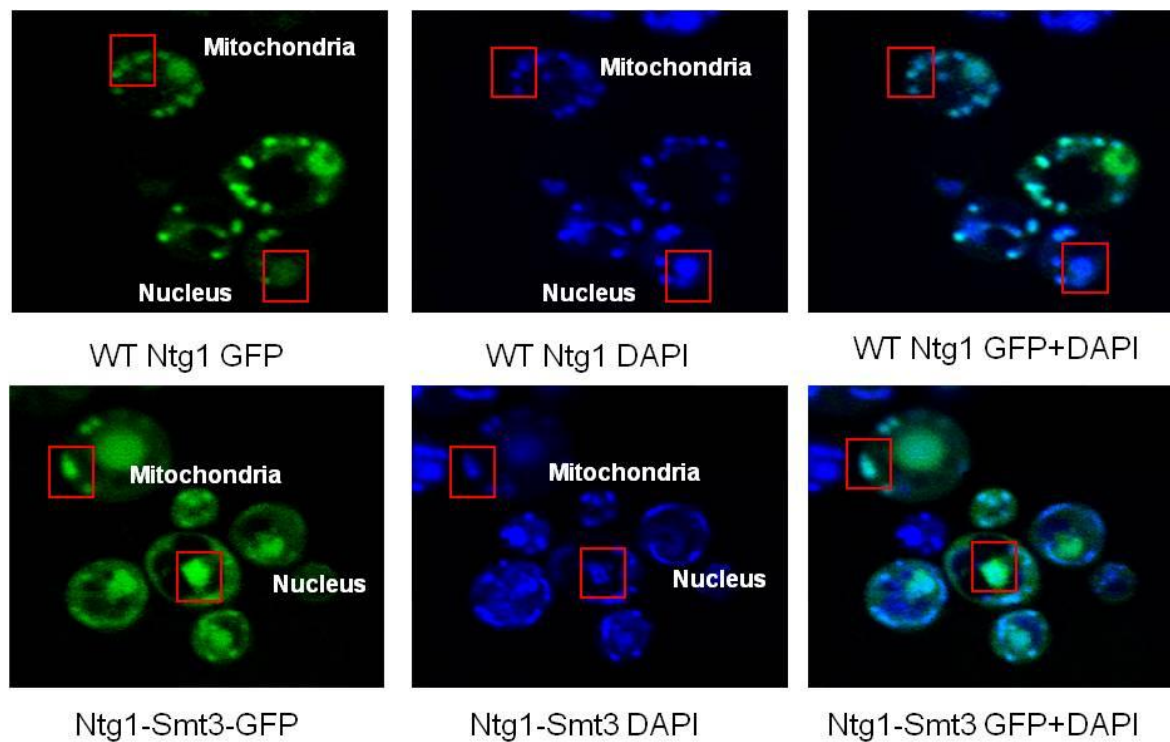


Figure 6

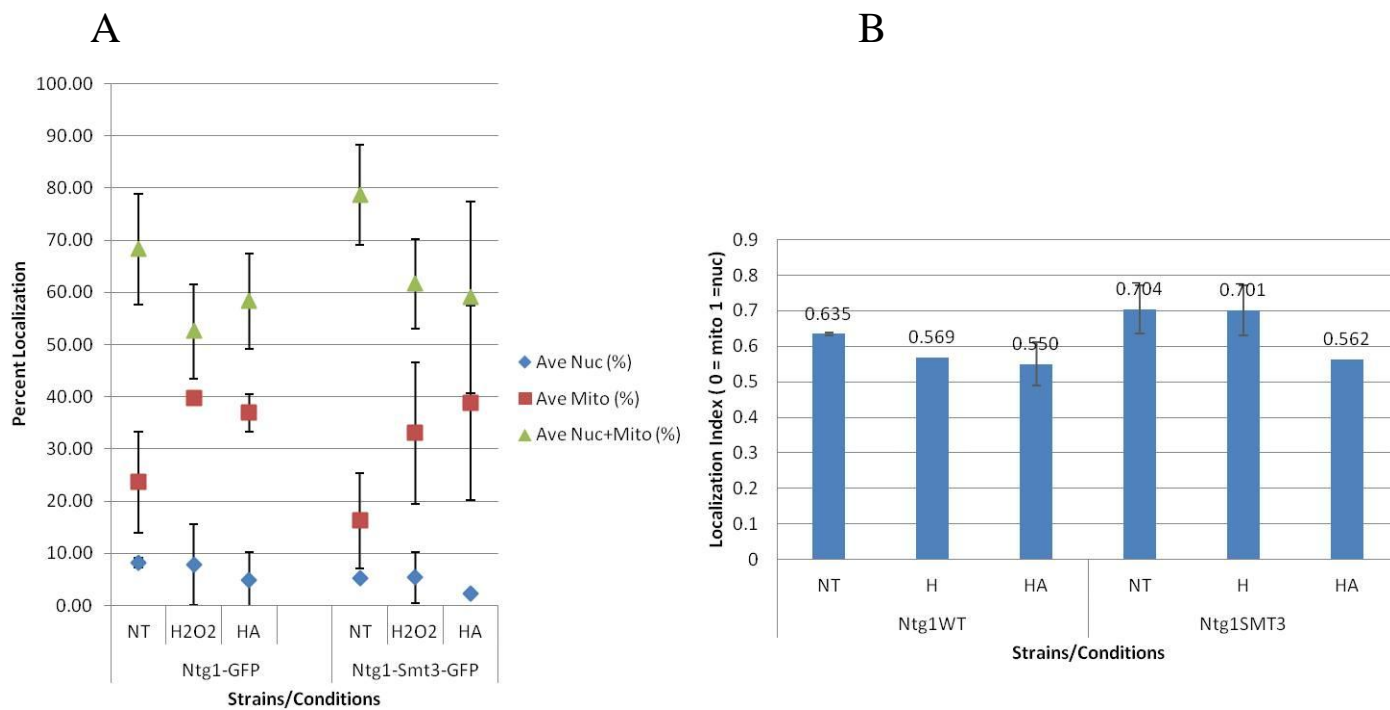


Figure 7

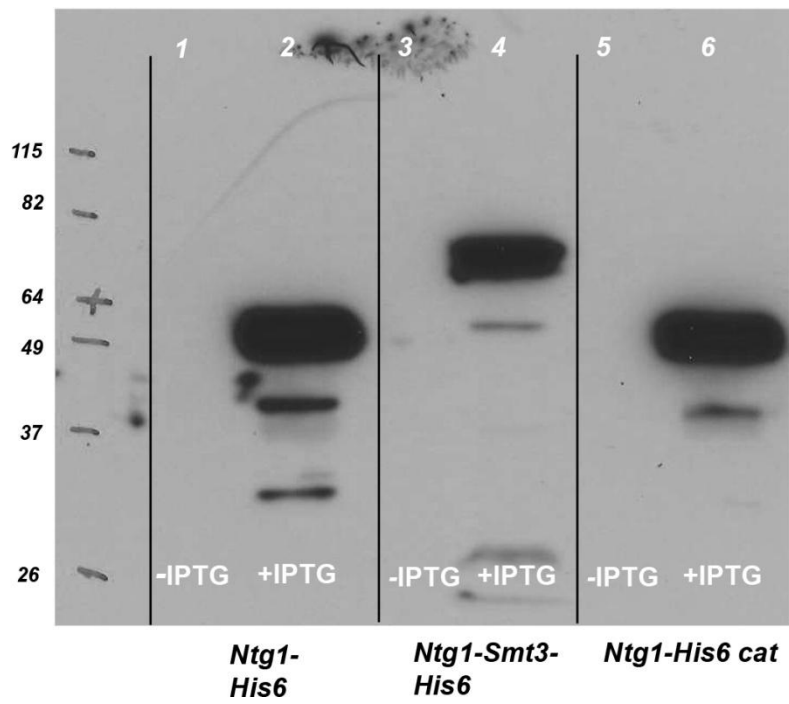


Figure 8

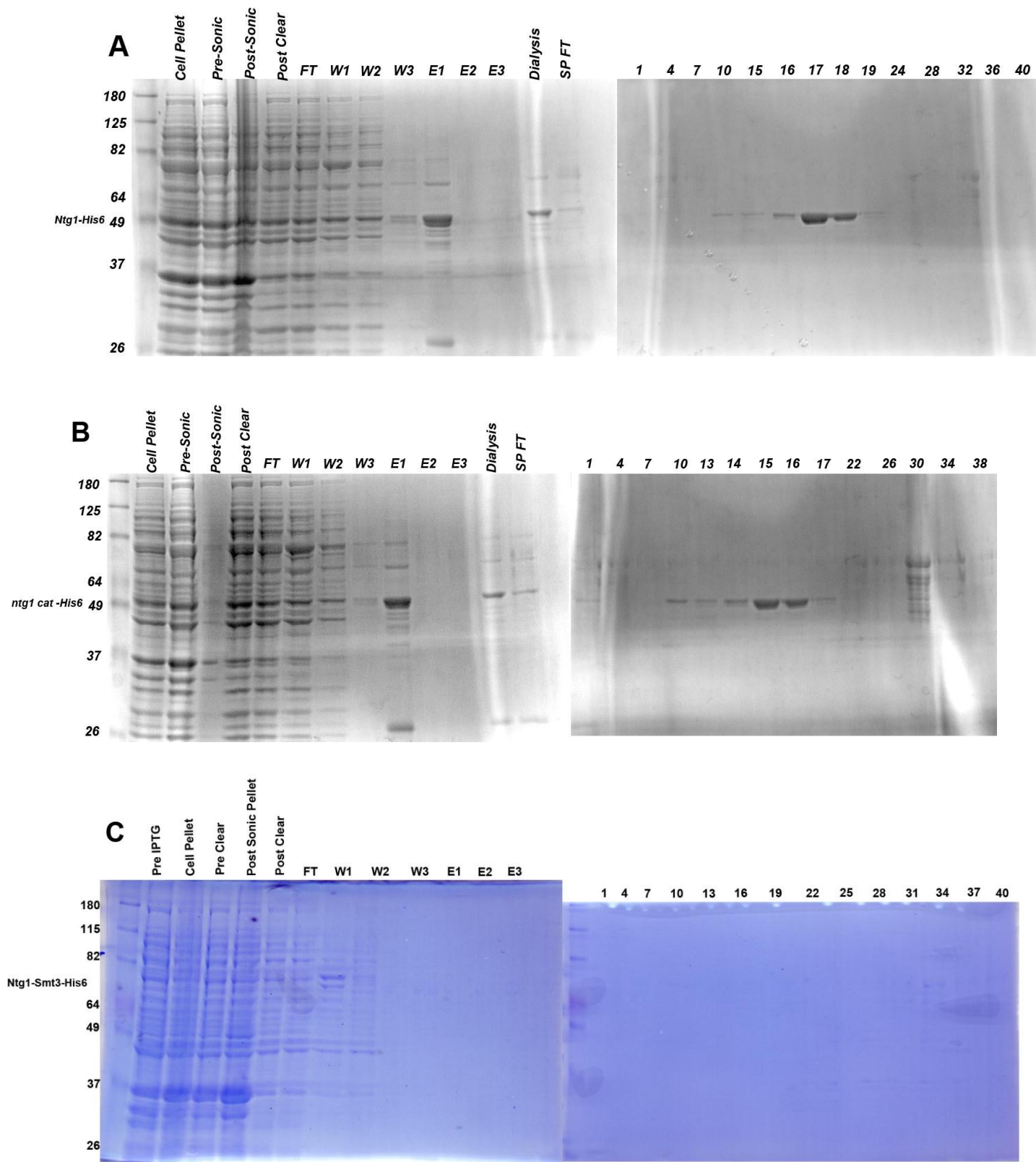


Figure 9

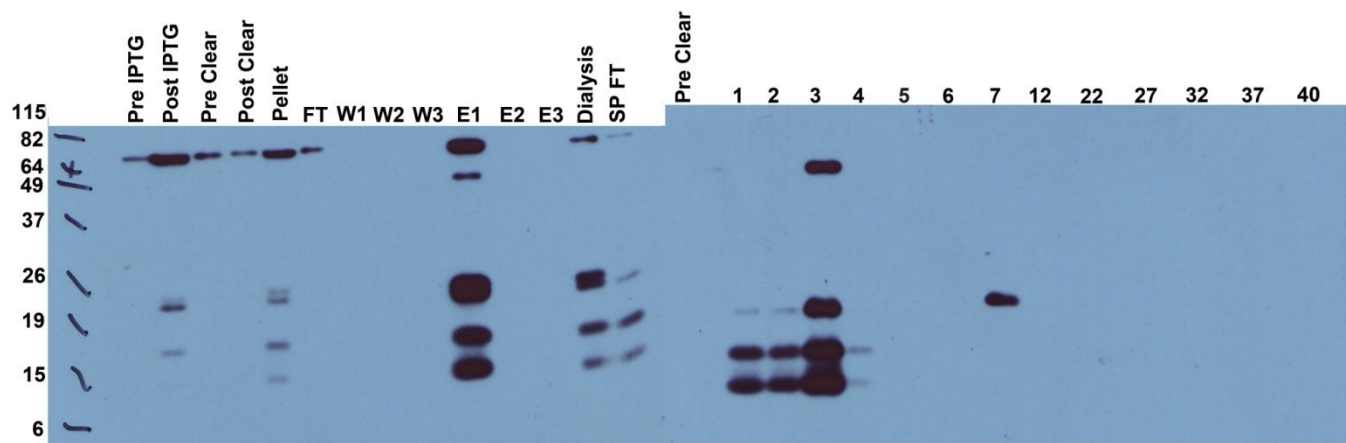


Figure 10

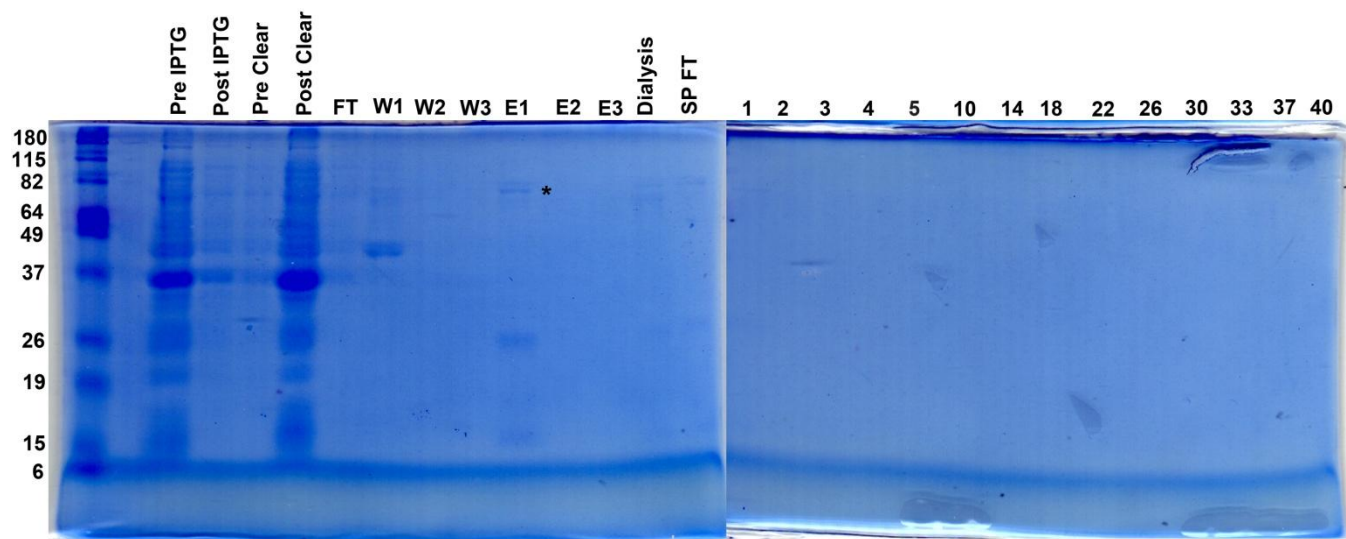


Figure 11

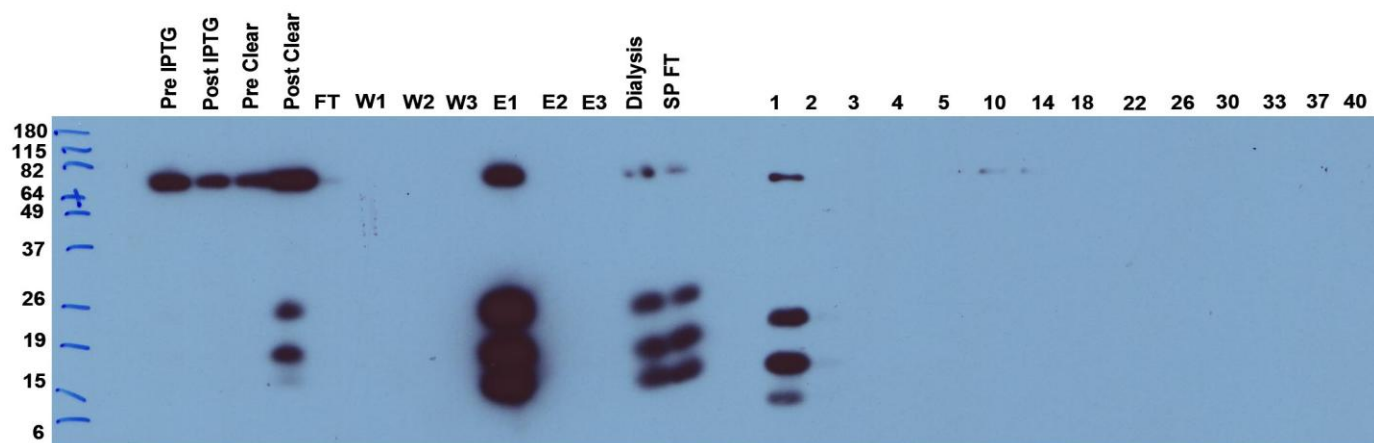


Figure 12

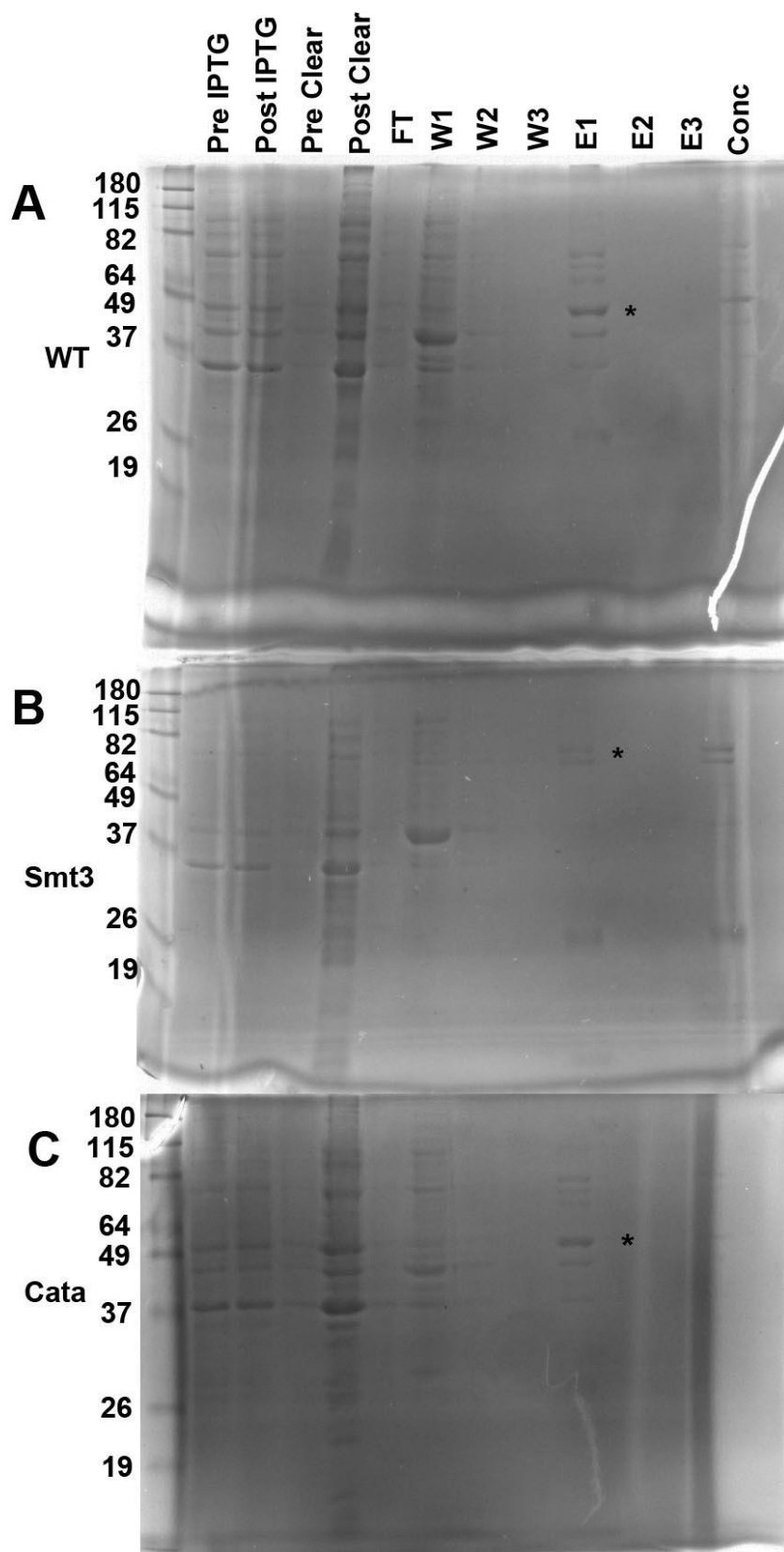


Figure 13

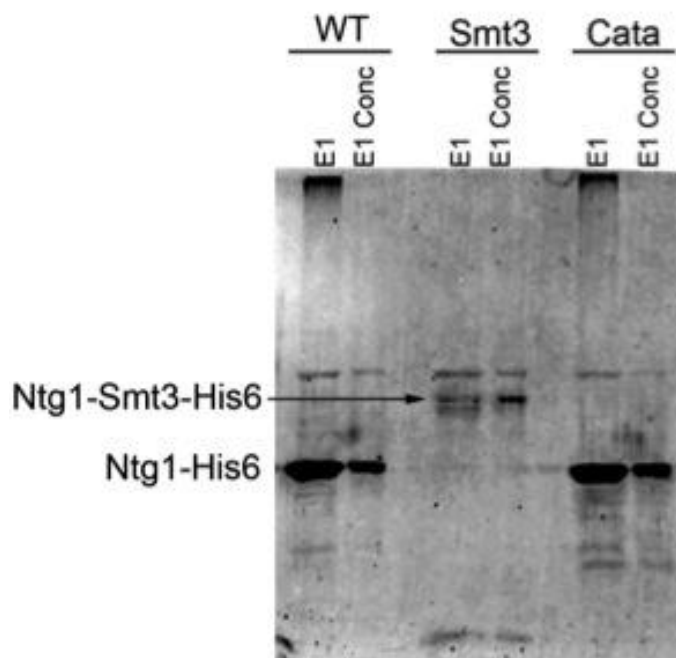


Figure 14

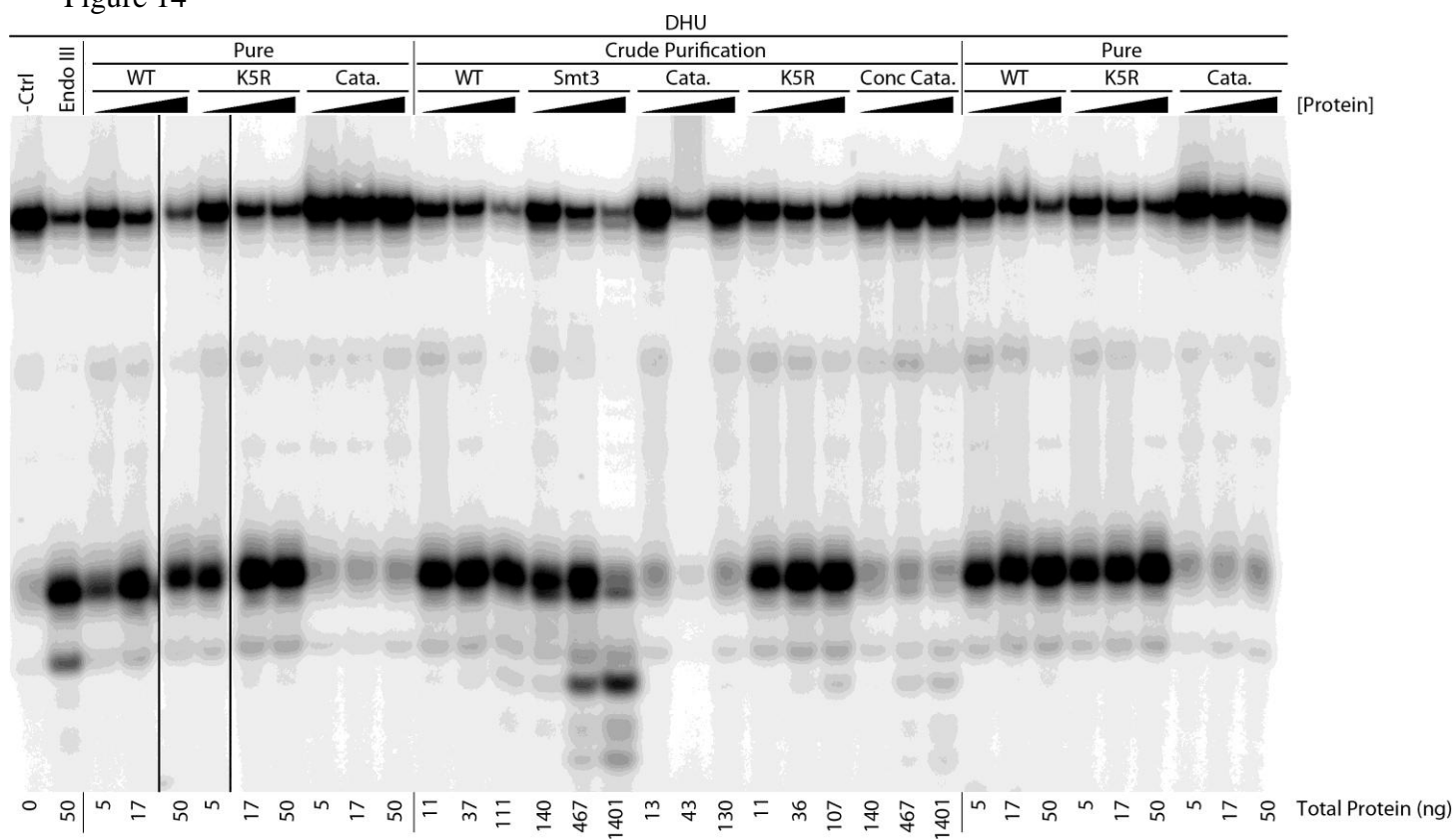


Figure 15

